Int. J. Heat Mass Transfer. Vol. 30, No. 4, pp. 699–706, 1987
Printed in Great Britain

0017–9310/87 $3.00 + 0.00
Pergamon Journals Ltd.

Mass transfer-controlled bubble growth during rapid decompression of a liquid

PARVIZ PAYVAR

Roy C. Ingersoll Research Center, Borg–Warner Corporation, Des Plaines, IL 60018, U.S.A.

(*Received* 5 *March* 1985 *and in final form* 23 *July* 1986)

Abstract—An analysis based on the integral method is presented for the solution of mass transfer-controlled bubble growth during a rapid decompression of a liquid–gas solution. Predicted results are in very good agreement with experimental measurements on an ethyl alcohol–CO_2 solution at 25 °C and initial pressures of 0.44–1.12 MPa. An outline of the way in which the bubble growth model could be combined with a bubble nucleation model to predict void fractions in one-dimensional two-phase flow passages is given. Specific results for bubble growth and void fraction calculations are presented for the flow of monoethanolamine–CO_2 solution at an initial pressure of 8.8 MPa and 150°C through a single-stage turbine and a five-stage reverse pump.

1. INTRODUCTION

THE STUDY in this paper was motivated by the desire to estimate void fractions between the inlet and outlet of various designs of hydraulic power recovery turbines. The liquids handled by these turbines, monoethanolamine and diethanolamine being typical examples, are at high pressures exceeding 10 MPa at the inlet and contain a high concentration of dissolved gases such as CO_2 and H_2S. As such liquids pass through the turbine, each fluid particle experiences a rapid pressure drop in time intervals typically ranging from 20 to 300 ms. This rapid decompression sets up a substantial concentration difference between the bulk of the liquid and the liquid–gas interface of any gas bubbles which may be present. The diffusion of gas from the liquid bulk into these gas bubbles causes them to grow and increase the void fraction. In addition, the gas bubbles grow as a result of the pressure drop itself. The analysis of the diffusion-controlled growth of gas bubbles is but one aspect of a complete model for the prediction of void fraction. Other elements of the model involve the mechanism of bubble generation, and *a priori* knowledge of the pressure–time history observed by the flowing fluid. For the former, a number of results such as the bubble frequency and the number of favorable sites for bubble generation as reported in the literature of nucleate boiling is used. For the latter, a pressure–time history is assumed *a priori*. But in principle, after the void fraction distribution between inlet and outlet of the fluid passage has been calculated, an iterative procedure could be used to recalculate the pressure–time history.

The main emphasis in the present paper will be on the bubble growth model in a rapid decompression for liquids containing large amounts of dissolved gases and the experimental verification of the model. Numerous papers have been published on bubble growth on both heat transfer-controlled and diffusion-controlled cases. The underlying conservation equations are described in detail in the classic paper by Scriven [1]. Arpaci *et al.* [2] have studied the dynamics of gas vapor bubbles in binary systems and have considered the combined effect of mass and heat transfer. The liquid pressure p_∞, however, was treated as constant in their study. Cha and Henry [3] have presented a solution of the diffusion equation in spherical coordinates valid for cases in which the convection set up by the growth of the bubble is negligible. This tacity implies that the decompression occurs over a relatively long time interval. The results that they present and the experimental data which they use for comparison are both for cases where the decompression time is of the order of 40 s. In the practical situations of interest in this study, convection effects are not negligible. Rosner and Epstein [4] present a method of solution of the diffusion equation based on integral methods which takes into account the effect of convection. While it is possible to employ numerical methods of solution of the diffusion equation, their method was deemed sufficiently accurate for the objectives of the present study. In the following sections, the basic equations underlying the model and the method of solution are described. Results obtained in the application of the model to particular situations are then presented and compared to experimental results. An outline of the way the method may be combined with a bubble generation model and a pressure–time history to predict void fractions in one-dimensional flow is also presented.

NOMENCLATURE

A	solid surface area in contact with fluid
b	supersaturation parameter
C	concentration of dissolved gas
D	diffusion coefficient
D_b	bubble departure diameter
F	function defined by equation (18)
f	bubble departure frequency
H	Henry's constant defined by equation (15)
N	number of nucleation sites per unit area
P	dimensionless pressure
P_{rr}	normal stress
p_g	gas pressure inside bubble
p_v	vapor pressure of liquid
$p_{L\infty}$	ambient pressure of liquid
$\dot{Q}_g$	volume flow rate of gas
R	bubble radius
R_g	gas constant
R_i	initial bubble radius
T	temperature
t	time
t_e	residence time
u	radial component of liquid velocity
v	dummy variable of integration
X	ratio of concentration boundary layer thickness to radius
Y	dimensionless bubble radius.

Greek symbols

α	dimensionless parameter defined by equation (24)
β	dimensionless parameter defined by equation (28)
δ	concentration boundary layer thickness
η	variable defined by equation (29)
ν	kinematic viscosity of liquid
ρ	solution density
σ	surface tension
τ	dimensionless time.

Subscripts

1	time or section where a bubble is generated
e	exit
g	gas
i	initial
rr	radial direction
w	gas–liquid interface
∞	liquid bulk.

Superscripts

$\dot{}$	differentiation with respect to time.

2. MATHEMATICAL MODEL

Although many of the equations presented below are the same as those used in refs. [1–4], there are sufficient major differences such as the assumption of a variable gas density, the inclusion of the convection effect of the growing bubble on mass transfer rate, the use of a more general concentration profile in the mass transfer boundary layer, and a more accurate expression for the mass transfer boundary layer thickness to warrant a complete presentation of the governing equations.

Assuming the bubble to be spherical in shape throughout its growth period, the governing equations in spherical coordinates are as follows (see Fig. 1).

Continuity equation for the liquid phase

$$u(r) = R^2 u(R)/r^2. \tag{1}$$

Overall mass balance

$$\frac{\mathrm{d}}{\mathrm{d}t}\left(\frac{4}{3}\pi\rho_g R^3\right) = 4\pi R^2 \rho(\dot{R} - u(R)). \tag{2}$$

Substitution of equation (2) in equation (1) yields

$$u(r) = \frac{1}{r^2}\left[R^2\dot{R} - \frac{1}{3\rho}\frac{\mathrm{d}}{\mathrm{d}T}(R^3\rho_g)\right]. \tag{3}$$

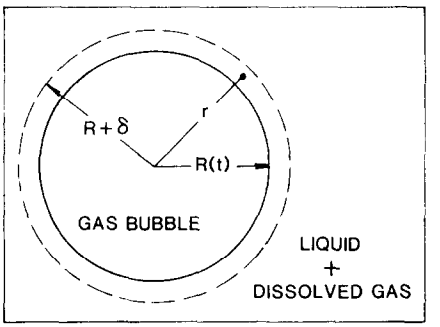

FIG. 1. Geometry and the coordinate system for a gas bubble in a liquid–gas solution.

The gas density ρ_g is assumed to obey the perfect gas law

$$\rho_g = \frac{p_g}{R_g T_g}. \tag{4}$$

Momentum equation. With the only non-zero velocity component being the radial velocity $u(r)$ in spherical coordinates, the momentum equation has the form

$$\frac{\partial u}{\partial t} + u\frac{\partial u}{\partial r} = \frac{1}{\rho}\frac{\partial P_{rr}}{\partial r} - 2\nu\frac{\partial^2 u}{\partial r^2} \tag{5}$$

where P_{rr} is the normal stress component given by

$$P_{rr} = p_g + p_v - \frac{2\sigma}{R}. \tag{6}$$

Integration of equation (5) from $r = R$ to ∞ and use of equation (6) gives the following equation relating the gas pressure inside the bubble to the ambient instantaneous liquid pressure surrounding the bubble

$$p_g = p_{L\infty} - p_v + \frac{2\sigma}{R} + (\rho - \rho_g)\left[R\dot{R} + \left(\frac{3}{2} + \frac{\rho_g}{2\rho}\right)\dot{R}_2 + 4\nu\frac{\dot{R}}{R}\right] - \left(\frac{5}{3} + \frac{\rho_g}{3\rho}\right)\dot{\rho}_g R\dot{R} - \left(\frac{\dot{\rho}_g^2}{18\rho} + \frac{\ddot{\rho}_g}{3}\right)R_2 - \frac{4\nu\dot{\rho}_g}{3}. \quad (7)$$

Equation (7) is the complete extended Rayleigh equation. It reduces to various more simplified forms used by other authors if the relevant simplifying assumptions are made. The effects due to viscous, surface tension, and liquid inertia have been shown by Birkhoff *et al.* [5] to be negligible provided that the initial bubble size is not extremely small. For the range of conditions covered in the present study, $p_{L\infty}(t)$ is the dominant term. After determination of R as a function of t, the total contribution of viscous, surface tension and inertia terms was estimated and turned out to be less than 1% of $p_{L\infty}(t)$. Therefore, we adopt these assumptions and the additional one that the liquid vapor pressure p_v is much smaller than the gas pressure p_g, the result is the simple equation

$$p_g = p_{L\infty}(t). \quad (8)$$

In the particular application in this paper interest is focused on bubble sizes of 10^{-3}–10^{-4} m in diameter initially in equilibrium at liquid pressures of at least 10 MPa dropping rapidly to 1–2 MPa in less than 1.0 s. The dominant term under the stated condition is $p_{L\infty}(t)$ given in equation (8). The use of equation (8), however, is purely a matter of convenience. In principle, if a particular application warrants a more accurate solution, the full equation (7) may be used at each stage of an iterative procedure to obtain p_g as a function of time.

Mass diffusion equation. The equation governing the variation of the dissolved gas concentration in the liquid surrounding the bubble is

$$\frac{\partial C}{\partial t} + u(r)\frac{\partial C}{\partial r} = \frac{D}{r^2}\frac{\partial}{\partial r}\left(r^2\frac{\partial C}{\partial r}\right) r \geq R. \quad (9)$$

Equating the rate of increase of the mass trapped in the bubble to the mass flow rate at the boundary in terms of the concentration gradient, one obtains

$$\frac{d}{dt}\left(\frac{4}{3}\pi\rho_g R^3\right) = \frac{D\rho}{\rho - C_w}\left(\frac{\partial C}{\partial r}\right)_{r=R} 4\pi R^2. \quad (10)$$

The boundary conditions for the diffusion equation are:

$$\text{at } r = R, \quad C = C_w \quad (11)$$

$$\text{at } r \to \infty, \quad C \to C_\infty \quad (12)$$

$$\text{at } t = 0, \quad C = C_\infty, r > R \quad (13)$$

$$\text{at } t = 0, \quad R = R_i. \quad (14)$$

Furthermore, it is assumed that at the interface between the gas and the liquid, thermodynamic equilibrium exists and that the equilibrium follows Henry's law

$$C_w = Hp_g. \quad (15)$$

Examination of solubility data for gas–liquid systems of the present study indicated that equation (15) could be used with a suitable value of H to express the relation between C_w and p_g. Following Rosner and Epstein [4], it is assumed that the transition from the concentration C_∞ in the liquid bulk to C_w at $r = R$ takes place in a boundary layer of thickness δ surrounding the bubble. Assuming a concentration profile of the form

$$\frac{c - c_\infty}{C_w - C_\infty} = \begin{cases} \frac{R}{r}\left[1 - \frac{r - R}{\delta}\right]^2, & R \leq r \leq R + \delta \\ 0, & r \geq R + \delta \end{cases} \quad (16)$$

and essentially retracing the steps outlined in ref. [4], one can show that

$$\frac{1}{4}\left(\frac{\delta}{R}\right)^2 + \left(\frac{\delta}{R}\right) - F = 0 \quad (17)$$

where F is given by the relation

$$F = \frac{C_\infty - \rho}{C_w - C_\infty}\frac{\rho_g}{\rho}\left[1 - \frac{\rho_{gi}}{\rho_g}\left(\frac{R_i}{R}\right)^3\right]. \quad (18)$$

Let $X = (\delta/R)$ and solve the quadratic equation (17) to obtain

$$X = 2[\sqrt{(1 + F)} - 1]. \quad (19)$$

In the above development equation (19) is preferable to that used by Rosner and Epstein [4] since the assumption $\delta/R \ll 1$ is not necessary.

Using equation (16), the concentration gradient at $r = R$ is obtained

$$\left(\frac{\partial C}{\partial r}\right)_{r=R} = -(C_w - C_\infty)\left(\frac{1}{R} + \frac{2}{\delta}\right). \quad (20)$$

Substitution of equation (20) in equation (10) yields after some simplification

$$\frac{1}{3}\frac{d}{dt}(\rho_g R^3) = \frac{D\rho(C_\infty - C_w)}{\rho - C_w} R\left(1 + \frac{2}{X}\right). \quad (21)$$

Even at the high pressures considered in the present investigation $C_w \ll \rho$ so that $\rho/(\rho - C_w) \simeq 1$.

To simplify the equations, introduce the dimensionless variables:

$$Y = \frac{R}{R_i} \quad (22)$$

$$\tau = \frac{t}{t_c} \quad (23)$$

$$\alpha = \frac{3DHR_gT_gt_c}{R_i^2} \quad (24)$$

$$P(\tau) = \frac{P_{L\infty}(t)}{P_{L\infty}(0)} \tag{25}$$

$$\tau_1 = \frac{t_1}{t_e} \tag{26}$$

$$P_1 = P(\tau_1) \tag{27}$$

$$\beta = HR_gT_g \tag{28}$$

$$\eta = \tau_1 + \frac{\tau - \tau_1}{2}(v + 1) \tag{29}$$

$$b = \frac{C_\infty}{Hp_{L\infty}(0)}. \tag{30}$$

Equation (21) may now be integrated from $t = t_1$ to t and cast in terms of the above dimensionless variables to give

$$Y^3(\tau_1, \tau) = \frac{P_1}{P(\tau)}\left[1 + \frac{\alpha(\tau - \tau_1)}{2}\int_{-1}^{1}\left(\frac{b}{P_1} - \frac{P(\eta(v))}{P_1}\right)Y(\tau_1, \eta)\left(1 + \frac{2}{X(\eta)}\right)dv\right]. \tag{31}$$

Equation (31) is an integral equation governing the growth of a gas bubble of initial radius R_i born at time t_i in a pressure field following the pressure–time history given by the function $p_{L\infty}(t)$. An assumed solution for Y is substituted on the right-hand side of equation (31) and a new value obtained for $Y(\tau_1, \tau)$. The procedure is repeated until satisfactory convergence. It was found that if one uses the value of Y due to just the pressure change effect and multiply that value by a factor slightly larger than 1, say 1.1, the procedure converges within 2–3 iterations. At each step X is calculated from equation (19) with F given by

$$F = \frac{P(\tau) - P_1 b/Y^3(\tau_1, \tau)}{\beta(b - P(\tau))}. \tag{32}$$

3. THEORETICAL RESULTS

Figure 2 shows a typical pressure–time history experienced by a liquid particle as it passes through a five-stage reverse pump used to recover power from a stream of high pressure liquid such as monoethanolamine. The initial pressure is about 8.8 MPa and the temperature is 150 °C. The residence time of the liquid in the machine is approximately 340 ms. The stream at the inlet contains a large concentration of dissolved CO_2. Henry's constant H and the diffusion coefficient D are estimated to have the values

$$H = 1.2 \times 10^{-4}\,\mathrm{m}^{-1}$$

$$D = 1.0 \times 10^{-8}\,\mathrm{m}^2\,\mathrm{s}^{-1}.$$

Bubble growth histories calculated by using the mathematical model presented in the previous section are shown in Figs. 2 and 3 for initial radii of 4×10^{-5} and 1.0×10^{-4} m, respectively. In each figure, growth

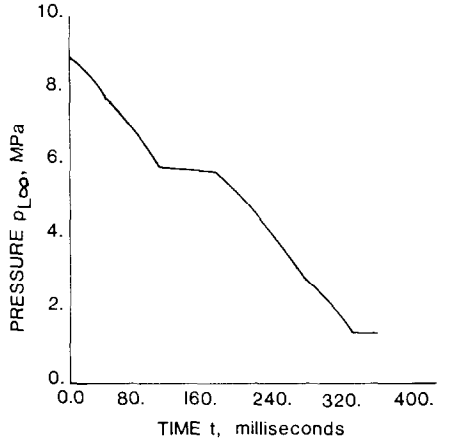

FIG. 2. Typical pressure variation in a five-stage reverse pump.

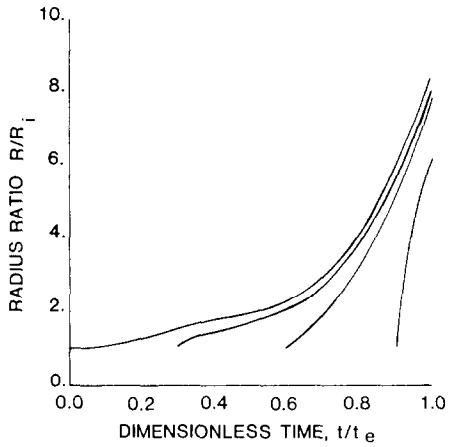

FIG. 3. Growth of bubbles generated at various locations with an initial radius of 4×10^{-5} m, $t_e = 340$ ms.

histories are shown for bubbles generated at $\tau = 0$, 0.3, 0.6 and 0.9. Two important observations may be made regarding these results. First, for bubbles generated near the inlet (small values of τ) the growth is initially very slow but accelerates as the bubble travels downstream. The reason for this behavior is that as the bubble travels downstream the pressure drops causing the concentration difference of the dissolved gas in the bulk and that at the liquid–gas interface to increase rapidly. The contribution of the pressure drop itself in causing the bubble to grow even in the absence of mass transfer is also greatest near the outlet region. For bubbles generated near the outlet, the concentration difference is already large causing rapid mass transfer-controlled bubble growth. Second, the growth of bubbles is much faster for smaller bubbles than for large bubbles. The main reason for this phenomenon is the thinner mass transfer boundary layer thickness associated with bubbles of smaller initial radius. We now turn to similar results for a single-stage power recovery turbine with a residence time of only 20 ms for the fluid particles.

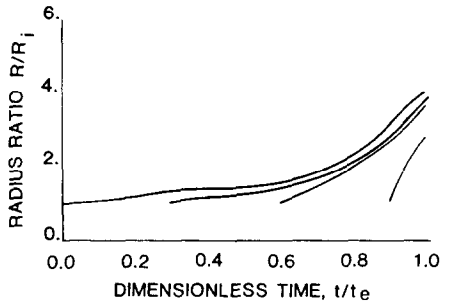

FIG. 4. Growth of bubbles generated at various locations with an initial radius of 1×10^{-4} m, $t_e = 340$ ms.

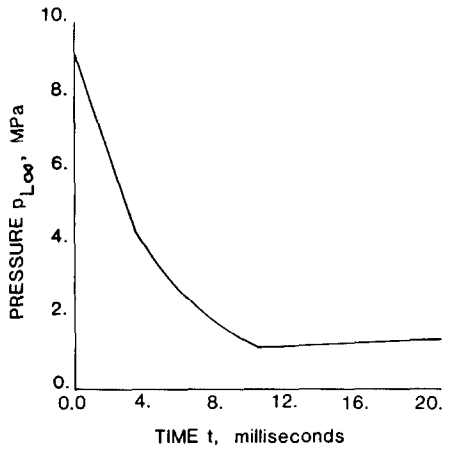

FIG. 5. Typical pressure variation for a single-stage turbine.

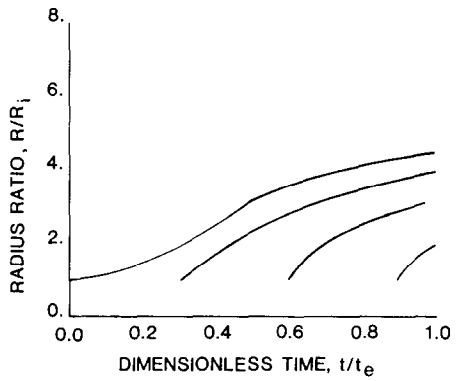

FIG. 6. Growth of bubbles generated at various locations with an initial radius of 4×10^{-5} m, $t_e = 20$ ms.

Figure 5 shows the pressure–time history used in the bubble growth calculations for a single-stage high speed power recovery turbine. Figures 6 and 7 show the bubble growth history for initial radii of 4.0×10^{-5} and 1.0×10^{-4} m, respectively. Trends are similar to those shown in Figs. 3 and 4 for the 340 ms residence time. An additional observation may now be made, however, by a comparison of the two sets of results. The bubble growth ratios for the 20 ms residence time are much smaller than the corresponding ones for 340 ms residence time. This is a direct

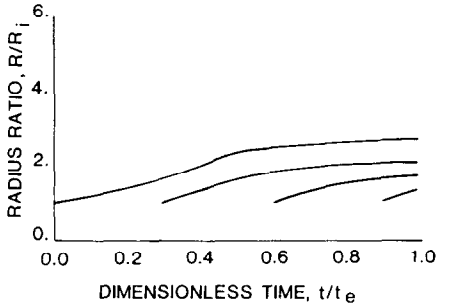

FIG. 7. Growth of bubbles generated at various locations with an initial radius of 1×10^{-4} m, $t_e = 20$ ms.

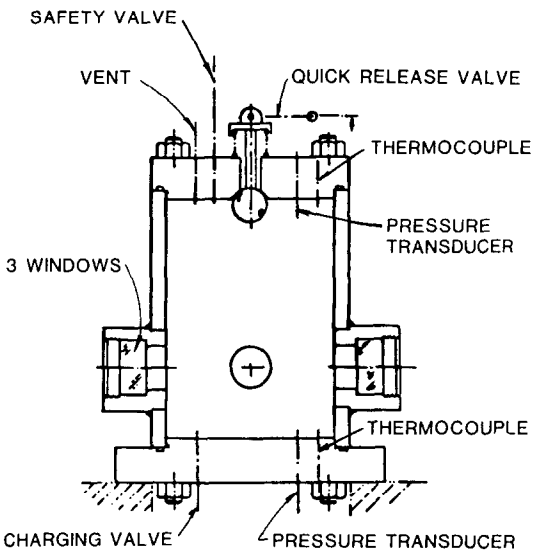

FIG. 8. Schematic diagram of test chamber for bubble growth experiments.

result of the importance of mass transfer-controlled bubble growth which is larger for the larger residence time. The equilibrium bubble sizes must be identical for the two cases because initial and final pressures are the same.

4. EXPERIMENTAL VERIFICATION OF THE BUBBLE GROWTH MODEL

Figure 8 shows the test chamber of the apparatus used for the experimental verification of the bubble growth theory presented above. The chamber is cylindrical in shape with a diameter of 0.2 and a height of 0.3 m. It was fitted with a quick release valve at the top, a safety valve, and a vent. At the bottom of the chamber, a charging valve was connected to a doughnut shaped distributor made of a porous metal. An injection needle was fitted at the bottom of the chamber and passing through the center of the doughnut shaped distributor in such a manner that its tip was visible through three transparent windows installed on the side walls. Two of the transparent windows were used for lighting the test chamber

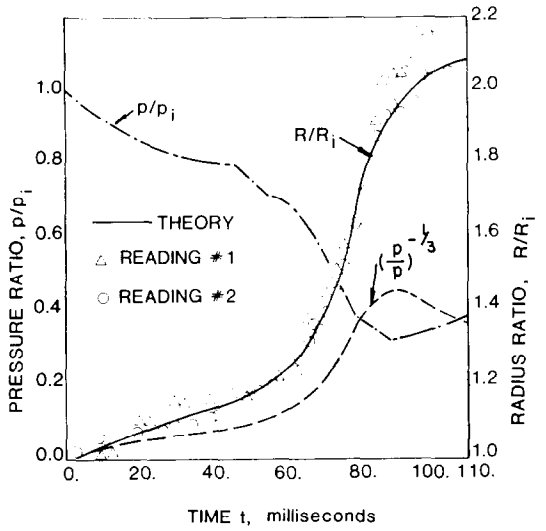

FIG. 9. Comparison of theoretical and experimental bubble growth histories. $R_i = 1.2 \times 10^{-4}$ m, $p_i = 0.44$ MPa, $T = 25$ °C, ethyl alcohol–CO_2 solution.

during the experiment, while the third was used for fitting a high-speed movie camera. Thermocouples and pressure transducers were installed at the top and the bottom of the chamber. The signal from the pressure transducer was stored in an oscilloscope for subsequent data reduction. Pure ethyl alcohol–CO_2 saturated solution was used in all the tests because of the good solubility of CO_2 in alcohol.

The test procedure consisted of filling the chamber with ethyl alcohol and then saturating it with CO_2 by connecting the distributor to a bottle of CO_2 and adjusting the pressure to the desired test pressure (0.44, 0.78, and 1.12 MPa). The porous metal distributor created a large number of small bubbles resulting in rapid (4 h) saturation times. The system was allowed to come to equilibrium for a period of 1 day. Any gas trapped in the upper portions of the chamber was then released through the vent and additional liquid was forced into the chamber to leave a minimal amount of undissolved gas in it. This was necessary for achieving short duration (50–120 ms) pressure relief. A single stream of bubbles was then injected into the chamber through the injection needle and the quick release valve was opened. A flash of light indicated the start of the event which was recorded by a high-speed camera at a speed of 3000 frames per second. Following the processing of the movie, it was projected on a large screen and the bubble diameter was measured from the first frame for every thirtieth frame. The known speed of the camera then allowed determinations of bubble radius ratio as a function of time.

Figure 9 shows a comparison of the results of the experiment at an initial pressure of 0.44 MPa, 25 °C, and an initial radius of 1.2×10^{-4} m with the predictions of the theoretical model. In the theoretical calculation, values of $H = 5.3 \times 10^{-4}$ m^{-1} and $D = 3.4 \times 10^{-9}$ m^2 s^{-1} were used. The pressure variation during the test is shown as the curve marked p/p_i. The curve marked $(p/p_i)^{-1/3}$ shows the expected bubble growth due to pressure drop alone with zero mass transfer. The solid curve shows the theoretically predicted bubble growth history including the effect of mass transfer which may be observed to be quite significant. The measured data is shown by the symbols and is in excellent agreement with the predicted results. In particular, the slow growth of bubbles in the initial period followed by a rapid growth near the end of the decompression is borne out by the experiment. Experiments at other pressures (0.78 and 1.12 MPa) produced similar results.

5. CALCULATION OF VOID FRACTION IN ONE-DIMENSIONAL FLOW

In this section, only a brief account will be given of the method by which the results of the bubble growth may be used to estimate the void fraction at various sections in a one-dimensional two-phase situation. A more comprehensive paper on this subject is in preparation which will be published elsewhere.

The following assumptions will be made to relate the void volume flow rate to the bubble growth model.

(1) The two-phase flow through the passage is homogeneous.

(2) The pressure distribution as seen by a flowing particle is known between inlet and outlet.

(3) The flow is steady with a specified total mass flow rate and inlet void fraction.

(4) The gas volume flow rate at any cross section of the passage originates from the following two sources:

(a) growth of bubbles existing at the inlet;

(b) growth of bubbles generated at all solid surfaces in contact with the fluid and situated upstream of the desired section.

Homogeneous nucleation in the bulk of the liquid will be neglected since this type of nucleation was not observed during the experimental verification of the bubble growth model. The last assumption in our model is given below.

(5) All bubbles existing at the inlet or generated at the walls are of uniform radius R_i.

The contribution of bubbles generated at an element of wall area dA situated upstream of a section to the gas volume flow rate at that section is then

$$d\dot{Q}_g = (N_f) \cdot \left(\frac{4}{3}\pi R^3\right) dA. \tag{33}$$

The total void volume flow rate is obtained by integrating equation (33) and adding the result to the void volume flow rate due to bubbles existing at the inlet. The growth of each bubble between its point of generation and the section at which void volume flow

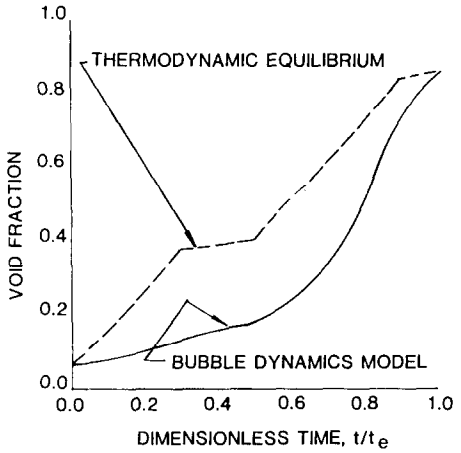

FIG. 10. Comparison of bubble dynamics and equilibrium void fractions, $t_e = 340\,\text{ms}$, $R_i = 1 \times 10^{-4}\,\text{m}$, monoethanolamine–$CO_2$ solution. Inlet void fraction = 0.07.

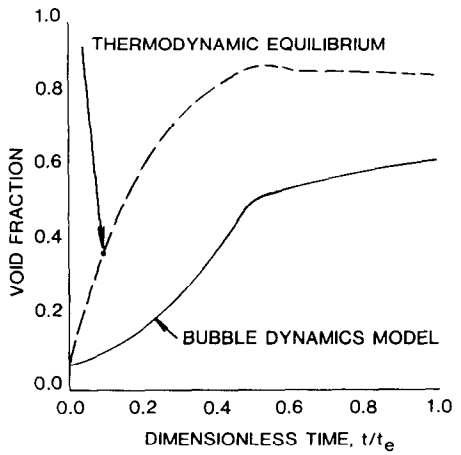

FIG. 11. Comparison of bubble dynamics and equilibrium void fractions, $t_e = 20\,\text{ms}$, $R_i = 1 \times 10^{-4}\,\text{m}$, monoethanolamine–$CO_2$ solution. Inlet void fraction = 0.07.

rate is being calculated is found by using the bubble growth model.

Figures 10 and 11 show the variation of void fraction between inlet and outlet for 340 and 20 ms residence times, respectively. The values for the number of favorable nucleation sites, N, and bubble departure frequency f were borrowed from the literature of boiling heat transfer. In particular, $N = 100{,}000\ \text{sites}\,\text{m}^{-2}$ and $fD_B = 0.06\,\text{m}\,\text{s}^{-1}$ were estimated from refs. [6, 7] for the present calculations.

Also shown on Figs. 10 and 11 are the thermodynamic equilibrium curves. It is observed from these two figures that for an inlet void fraction of 0.07, the void fraction for the five-stage reverse pump is everywhere below the thermodynamic equilibrium value but that the two values are very close at the exit. In contrast, the void fraction for the single stage machine is well below the thermodynamic equilibrium value and remains so throughout the flow passage. The main reasons are the smaller residence time and solid surface area in the single stage turbine.

6. CONCLUSIONS

(1) A theoretical model, based on an integral method of solution of the basic conservation equations, has been shown to predict results that are in very good agreement with experimentally measured values of mass transfer-controlled bubble growth.

(2) The model may be combined with suitable bubble nucleation and two-phase flow models to estimate the void fraction in two-phase flow passages.

Acknowledgements—The research work presented in this paper was carried out under project 4488 sponsored by Byron–Jackson Pump Division of Borg–Warner Corporation whose permission to publish this work is gratefully acknowledged. The contributions of Dr S. Gopalakrishnan of Byron–Jackson Pump Division through many helpful discussions is highly appreciated.

REFERENCES

1. L. E. Scriven, On the dynamics of phase growth, *Chem. Engng Sci.* **10,** 1–13 (1959)
2. V. S. Arpaci, J. A. Clark and P. S. Larsen, The dynamics of gas–vapor bubbles in binary systems, *Proc. R. Soc. London* (*A*) 50–63 (1965).
3. Y. S. Cha and R. E. Henry, Bubble growth during decompression of a liquid, ASME Paper No. 79-HT-73 (1979).
4. D. E. Rosner and M. Epstein, Effects of interface kinetics, capillarity and solute diffusion on bubble growth rates in highly supersaturated liquids, *Chem. Engng Sci.* **27,** 69–88 (1972).
5. G. Birkhoff, R. S. Margulies and W. A. Horning, Spherical bubble growth, *Physics Fluids* **1**(3), 201–204 (1958).
6. W. C. B. V. Ceumern-Lindenstjerna, Bubble departure diameter and release frequencies during nucleate pool boiling of water and aqueous sodium chloride solutions, *Heat Transfer in Boiling* (edited by E. Hahne and U. Grigull), Chap. 3, p. 66. Academic Press, New York (1977).
7. W. M. Rohsenow and H. Y. Choi, *Heat, Mass and Momentum Transfer*, p. 228. Prentice Hall, Englewood Cliffs, New Jersey (1961).

CROISSANCE DE BULLE CONTROLEE PAR LE TRANSFERT MASSIQUE PENDANT LA RAPIDE DECOMPRESSION D'UN LIQUIDE

Résumé—On présente une analyse basée sur une méthode intégrale pour la croissance d'une bulle contrôlée par le transfert massique pendant la décompression brutale d'une solution de gaz dans un liquide. Les résultats du calcul sont en très bon accord avec les mesures expérimentales faites sur une solution alcool éthylique–CO_2 à 25°C et des pressions initiales entre 0,44 et 1,12 MPa. On donne un moyen de combiner le modèle croissance de bulle avec un modèle de nucléation de bulle pour prédire les fractions de vide dans des écoulements diphasiques à passage unidirectionnel. Des résultats pour la croissance de bulle et le calcul de fraction de vide sont présentés concernant la solution monoéthanolamine–CO_2 à une pression initiale de 8,8 MPa et 150°C, à travers une turbine à un seul étage et une pompe à cinq étages.

STOFFÜBERGANGSKONTROLLIERTES BLASENWACHSTUM WÄHREND DER SCHNELLEN ENTSPANNUNG EINER FLÜSSIGKEIT

Zusammenfassung—Eine auf der Integralmethode basierende analytische Lösung für das stoffübergangskontrollierte Blasenwachstum während schneller Entspannung einer Flüssigkeits–Gas-Lösung wird vorgestellt. Die berechneten Werte stimmen sehr gut mit Meßergebnissen von Ethylalkohol–CO_2-Lösungen bei 25°C und Anfangsdrücken von 0,44 bis 1,12 MPa überein. Es wird ein Ausblick gegeben, wie das Blasenwachstumsmodell mit einem Blasenkeimmodell kombiniert werden kann, um Gasgehalte in eindimensionalen zweiphasigen Strömungsabschnitten zu berechnen. Spezielle Berechnungen von Blasenwachstum und Gasgehalt für Strömungen von Monoethanolamin–CO_2-Lösungen mit einem Anfangsdruck von 8,8 MPa und 150°C durch eine einstufige Turbine und durch eine fünfstufige umgekehrte Pumpe werden vorgestellt.

КОНТРОЛИРУЕМЫЙ МАССОПЕРЕНОСОМ РОСТ ПУЗЫРЬКОВ ПРИ РЕЗКОМ СНИЖЕНИИ ДАВЛЕНИЯ В ЖИДКОСТИ

Аннотация—Решение задачи контролируемого массопереносом роста пузырьков при резком снижении давления в смеси жидкость–газ анализируется на основании интегрального метода. Представленные результаты расчета хорошо согласуются с экспериментальными измерениями, проведенными с раствором этилового спирта–CO_2 при 25°C и начальном давлении от 0,44 до 1,12 МПа. Описан способ обобщения моделей роста пузырька и зародыше образования для расчета истинного объемного паросодержания в одномерном двухфазном течении в каналах. Представлены характерные результаты роста пузырьков и расчеты истинного объемного паросодержания для течения смеси моноэтаноламин–CO_2 при начальном давлении 8,8 МПа и температуре 150°C в одноступенчатой турбине и пятиступенчатом реверсивном насосе.